coatings

MDPI

Review

Restraining Surface Charge Accumulation and Enhancing Surface Flashover Voltage through Dielectric Coating

Jixing Sun *, Sibo Song, Xiyu Li, Yunlong Lv, Jiayi Ren, Fan Ding and Changwang Guo

School of Electrical Engineering, Beijing Jiaotong University, Haidian District, Beijing 100044, China; 20121485@bjtu.edu.cn (S.S.); 19126132@bjtu.edu.cn (X.L.); 20126177@bjtu.edu.cn (Y.L.); 19126147@bjtu.edu.cn (J.R.); 20126129@bjtu.edu.cn (F.D.); 19126107@bjtu.edu.cn (C.G.)
* Correspondence: sanyou345@163.com; Tel.: +86-15801067328

Abstract: A conductive metallic particle in a gas-insulated metal-enclosed system can charge through conduction or induction and move between electrodes or on insulating surfaces, which may lead to breakdown and flashover. The charge on the metallic particle and the charging time vary depending on the spatial electric field intensity, the particle shape, and the electrode surface coating. The charged metallic particle can move between the electrodes under the influence of the spatial electric field, and it can discharge and become electrically conductive when colliding with the electrodes, thus changing its charge. This process and its factors are mainly affected by the coating condition of the colliding electrode. In addition, the interface characteristics affect the particle when it is near the insulator. The charge transition process also changes due to the electric field strength and the particle charging state. This paper explores the impact of the coating material on particle charging characteristics, movement, and discharge. Particle charging, movement, and charge transfer in DC, AC, and superimposed electric fields are summarized. Furthermore, the effects of conductive particles on discharge characteristics are compared between coated and bare electrodes. The reviewed studies demonstrate that the coating can effectively reduce particle charge and thus the probability of discharge. The presented research results can provide theoretical support and data for studying charge transfer theory and design optimization in a gas-insulated system.

Keywords: metal particles; high-voltage power transmission; coating; insulator; movement characteristics

Citation: Sun, J.; Song, S.; Li, X.; Lv, Y.; Ren, J.; Ding, F.; Guo, C. Restraining Surface Charge Accumulation and Enhancing Surface Flashover Voltage through Dielectric Coating. *Coatings* **2021**, *11*, 750. https://doi.org/10.3390/coatings11070750

Academic Editor: Jaichan Lee

Received: 20 May 2021
Accepted: 17 June 2021
Published: 22 June 2021

1. Introduction

The importance of insulation breakdown and discharge caused by conductive particles in gas-insulated systems has attracted industrial attention. Understanding conductive particle charging, movement, and charge transfer is essential since these factors are important for designing gas-insulated systems, maintaining equipment, and developing insulation detection methods [1–8].

Theoretical and experimental research on the characteristics of conductive particle movement emerged with the development of gas-insulated switchgear (GIS) and gas-insulated power transmission lines (GILs). Since the advancement of SF_6 application in the mid-1960s, Western European countries (BBC of Switzerland and Delle of France) and Japan have directed more attention to GIS development. The Soviet Union and China completed 110 kV GIS research and trial production in the early 1970s; their initial research focused on withstand tests [9–16] and test methods [17–19].

As the power level increases, the movement of metal particles becomes the main factor affecting the internal insulation of GIS/GILs. Figure 1 (investigated by China Electric Power Research Institute in 2015) shows different possible causes of GIS failures, of which about 20% are related to metal particles [20–22]. The particle movement mechanism has been extensively researched through modeling. When the voltage level is higher than 500 kV, gas insulation failure in a GIL is mainly caused by metal particles. According to the statistics on gas-insulated system failures reported in China over the past decade [21],

particle suppression has become the primary factor to consider when designing the internal structure of gas-insulated equipment [3–15].

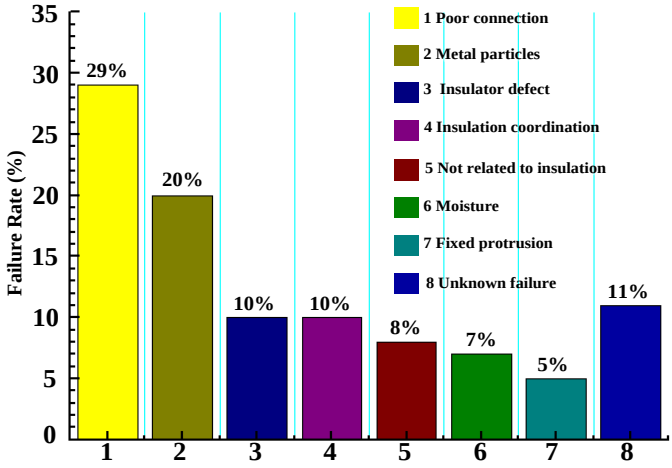

Figure 1. Probability of various causes of GIS failures.

The charge transfer and defects/deterioration due to conductive particles in gas-insulated systems were studied in the early 21st century through modeling. M. M. El Bahy et al. analyzed conductive particle charging on the electrode surface and coating surface to investigate the effects of the particle shape and electric field distribution on the charging characteristics [16]. The conductive particle motion behavior and collision characteristics in a wedge-shaped, slightly uneven electric field were numerically studied in a coupled manner to explore the gas-insulated system's structural and field distribution characteristics and the conductive particle motion law near the insulating support [10]. In addition, particle charging behavior and electrical conduction were studied to verify the efficacy of the insulating support structure. UHV transmission and transformation projects are being conducted internationally as power system globalization accelerates. However, further studies on conductive particle charging and movement on bare and coated electrode surfaces are necessary to gain a better understanding of charge transfer, which is valuable information for designing high-voltage equipment and optimizing withstand voltage test methods.

This paper reviews and summarizes the research progress of experimental work on the movement characteristics of conductive particles, associated models, and the inhibitory effect of electrode coating on surface particle charging. The current issues and problems involving gas-insulated switchgear and transmission line equipment in power systems are also analyzed. These analyses, together with theoretical developments of conductive particle charge transfer, can lay the foundation for future studies on electric conductor charging and gas discharge theories, providing a theoretical basis for GIS and GIL engineering design, defect detection, and the development of insulation test methods.

2. Charging Process of Conductive Particles on the Electrode Surface

Analyzing the force and movement of particles requires studying the charging process of conductive particles on the electrode surface and its influencing factors and rules [9–13]. The charging of conductive particles is explored from the following three aspects: the conductive particle charge in a high-voltage electric field, the influence of surface-coating materials on the amount of charging, and the impact of the charging process.

2.1. Charging Mechanism of Conductive Particles on the Bare Electrode Surface

Under an electric field, the metal particle surface on the ground electrode generates an electric charge. N. N. Lebedev et al. initially calculated the charge of spherical metal particles in a uniform electric field [11]. A. T. Pérez et al. confirmed their conclusion in

subsequent work. In a uniform electric field, the charge of metal particles is proportional to the area of the particles and the electric field intensity, expressed as [23,24]:

$$q_{\pm} = 2\pi^3 r^2 \varepsilon_0 \varepsilon_1 E/3 \quad (1)$$

where $q_{\pm}$ is the charge carried by spherical conductive particles, C; r is the radius of the spherical conductive particle, mm; ε_0 is the absolute dielectric constant, $\varepsilon_0 = 8.85 \times 10^{-12}$ F/m; ε_1 is the relative dielectric constant of the gas in the space; and E is the electric field intensity, kV/cm.

The orientation (horizontal or vertical) changes the calculation of linear particle charge. When conductive particles are placed horizontally, the carried charge q_{wire} is [25]:

$$q_{\text{wire}} = 2\pi\varepsilon_0 \varepsilon_1 rlE \quad (2)$$

When metal particles are oriented vertically, the carried charge q_{wire} is [25]:

$$q_{\text{wire}} = \frac{\pi\varepsilon_0 \varepsilon_1 l^2 E}{ln(2l/r) - 1} \quad (3)$$

In Equations (2) and (3), r is the cross-sectional radius of the wire conductive particle, mm; ε is the permittivity of free space; l is the length of the metal particle, mm; and E is the electric field intensity, kV/cm.

Table 1 shows the equivalent charges for conductive particles in other shapes.

Table 1. Charges of metal particles in uniform and slightly uneven electric fields.

Particles	**Sphere (Radius *r*)**	**Hemisphere (Radius *r*)**	**Semi-Ellipsoid (Radius *r*, Length *l*)**
Charge	$6.57\pi\varepsilon r^2 E$	$3\pi\varepsilon r^2 E$	$\frac{\pi\varepsilon l^2 E}{\ln(2l/r) - 1}$
Particles	Linear Particles (Radius r, and Length l)	Half Cylinder (Radius r, and Length l)	Thin Foil (Area S (Small), and Height h)
Charge	$2\pi\varepsilon rlE$	$4\pi\varepsilon rlE$	εSE

2.2. Mechanism of the Particle Charging Process on a Coated Surface

When the electrode surface is coated with a film, the charging time of metal particles increases, or the charge decreases accordingly. After coating, there are three main mechanisms of particle charging on the surface: (1) the surface of the medium has a charge, and the particles are charged by contact with the electrode film; (2) the particles are charged by the electric current in the medium; (3) the discharge of particles is based on the micro-discharge between the particles and the medium. Reference [16] shows that after the DC system is coated, the particle charge is essentially generated by the film's conduction. C. Li et al. established a conductive and micro-discharge model and calculated the charge of metal particles using the different models [2,12]. After comparing their results with measured values, they concluded that both charging mechanisms exist when the electrode is coated. Additionally, Y. Khan et al. determined the primary mode of particle charging by testing whether the gas pressure alters the intensity of the particle lifting field [26]. Specifically, if the SF_6 gas pressure has little influence on the lifting field intensity, then conduction is the primary driving mechanism of coated particles; when SF_6 is more influential, the primary driving mechanism is micro-discharge.

As reported in references [27,28], the coating reduces the particle charge and changes the electric field distribution around the particles, increasing the field intensity between the particles and the film. Furthermore, the charge analysis includes the Coulomb force, gravity, friction force, the viscous resistance of air, and the electric field gradient force [18]. Therefore, the relationship between the initial voltage of particle movement and the initial

particle position is calculated according to the force analysis and the motion equation, and the charge is estimated. By introducing the charge coefficient for the coated electrode surface, the charge of coated particles is:

$$q_{\pm\text{film}=}\xi q_{\pm\text{bare}} \tag{4}$$

where $q_{\pm\text{bare}}$ is the charge when the electrode surface is not coated, and ξ is the charge coefficient.

J. Wang et al. proposed a charging model for metal particles with a coated electrode under DC stress [26]. Since the coating does not affect the final charge of the particles, the calculation formula for the charge of coated particles is:

$$q_{\text{coated}}(t) = \int_0^t i_{\text{charge}} dt = q_{\text{bare}}\left(1 - e^{-\frac{t}{\tau}}\right) \tag{5}$$

where i_{charge} is the particle charging current, τ is the time-varying characteristic of the particle charging current, and t is the particle charging time.

The above formula shows that as absorption develops during the polarization process, the interface charge increases. Furthermore, the particle charge finally stabilizes, and $q_{\text{concluded}}(\infty) = q_{\text{bare}}$. This proves that the coating measures only extend the charging time compared to the bare electrode and do not affect the final charge.

When DC voltage is applied to the upper plate and $t = 0$, the overall electrode model is equivalent to a double-layer dielectric capacitor. At this point, the particles are charged due to current conduction. Based on the research conclusion about the accumulation and dissipation of the insulator surface charge, the conduction current of the particles comprises the electrical conduction current of the insulating film. C_1 is the capacitance between the metal particles near the gas medium and the upper plate, and C_2 is the capacitance between the insulating film-side particles and the insulating film (see the following expression) [26].

$$C_1 = \frac{2\pi^3 \varepsilon_0 \varepsilon_1 r^2}{3d_0} \tag{6}$$

$$C_2 = \frac{\varepsilon_0 \varepsilon_1 S}{3d_1} \tag{7}$$

where d_0 is the distance between the electrodes, mm; d_1 is the distance between the insulating film, mm; S is the contact area between the metal particles and the lower electrode plate; and r is the radius of the spherical conductive particle, mm.

The particle charging current is:

$$i_c(t) = \frac{C_1 U_0}{R_2(C_1 + C_2)} e^{-\frac{t}{\tau}} \tag{8}$$

where R_2 is the equivalent resistance on the insulating film side, U_0 is the voltage of the ideal power supply near the gas, τ is the time-varying characteristic of the particle charging current, and t is the particle charging time.

Through time integration of the particle charging current, the particle charge $q_c(t)$ is obtained as follows:

$$q_c(t) = q_0\left(1 - e^{-\frac{t}{\tau}}\right) \tag{9}$$

where q_0 is the particle charge under the bare electrode, τ is the time-varying characteristic of the particle charging current, and t is the particle charging time.

2.3. Experimental Study of Electrode/Coating Surface Particle Charging

The Faraday cup method is used to measure the particle charge with electrode surface charging [27–29], as shown in Figure 2. When the particle lifts off vertically from the surface due to the electric field, it is also moved horizontally by air currents. When it drops into the

Faraday cup and collides with the bottom, the charge can be measured by a coulombmeter since it contains an integrated circuit design; the charge is calculated by the impulse current, and then the total charge of particles is output.

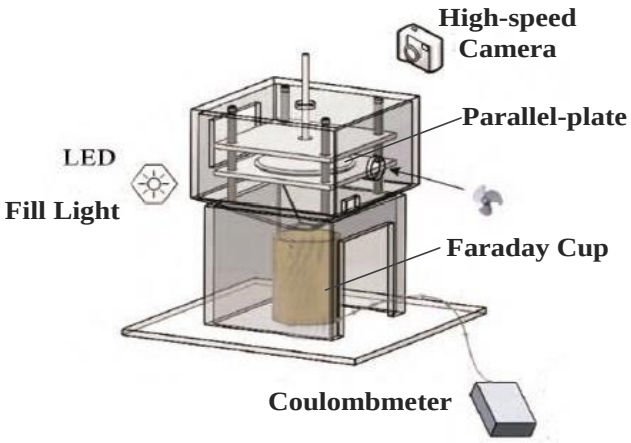

Figure 2. Faraday cup test system.

In Figure 3, the straight line is the theoretical charge. With bare electrodes, the measured charge is generally lower than the theoretical value. The reason is that when particles are blown off, a small part of the charge is lost as they collide with the organic glass [30].

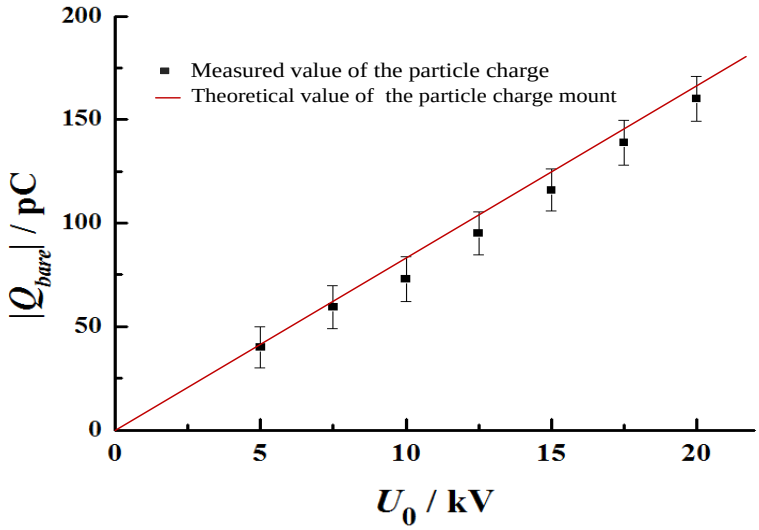

Figure 3. Charge of metal particles on the bare electrode.

L. E. Lundgaard et al. used anodized aluminum as the electrode coating material in experiments [31,32]. The particle charge was the same as that of the bare electrode. Jia et al. coated the electrode surface with a 100 μm thick polyethylene terephthalate (PET) film and calculated the particle charge to be about 30–60% of that obtained when the electrode was not coated based on the starting voltage of the particles under a wedge-shaped plate. Moreover, Y. Khan et al. used high-speed cameras to capture images of moving particles [8,25,26,32]. After processing the images, they obtained the instantaneous displacement of particle motion and calculated its acceleration. As a result, the charge can be calculated by inversion (see Table 2).

Table 2. Charges on the surface of bare and coated electrodes.

SF_6 Gas Pressure, p, MPa	Charge q/pC	
	q_{bare}	q_{film}
0.1	−152	−78.71
0.2	−220	−106.93
0.3	−258	−130.55

References [32–35] describe particle charging based on the new relationship between particle charge and the electric field force and field strength established in the Parekh model. After coating and before the field strength reaches the critical value at which micro-discharge occurs between the particles and the film, the particles are uncharged. When the field strength exceeds the critical value, the particle charge increases rapidly, but it is still less than the charge of bare electrode particles under the same field strength (see Figure 4) [19,23,24].

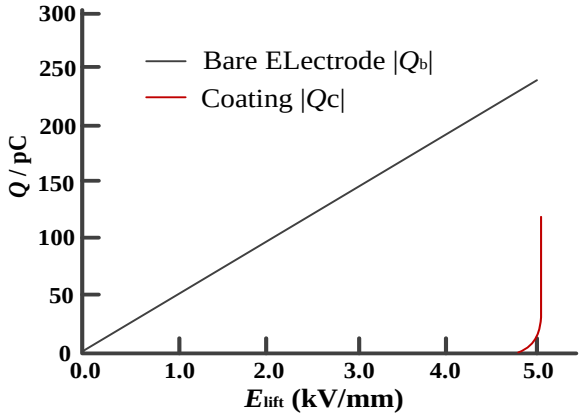

Figure 4. Relationship between electric charge and field strength.

However, M. Runde et al. hypothesized that electrostatic adsorption occurs between coated particles and the surface of the insulating film, so the higher initial voltage overcomes the electrostatic force instead of resulting in reduced particle charge [31]. The coating only increases the time required for the particle to obtain the charge without affecting its final charge (see Table 3).

Table 3. Charges of particles (r = 0.5 mm) at different times with different film thicknesses (20 kV).

Time t/min	Charge q/pC			
	q_{bare}	q_{film} (25 μm PET)	q_{film} (50 μm PET)	q_{film} (100 μm PET)
1	−221	−116	−61	−20
3	−221	−170	−151	−130
5	−221	−183	−180	−176

3. Movement Process of Conductive Particles

3.1. Lifting Process of Charged Conductive Particles

After being charged, metal particles move under the electric field force. They are affected by the electric field gradient force, gas drag force, and friction force during their movement [31–38].

Table 4 shows the instant force expression on the surface of metal particles.

Table 4. Surface force on metal particles.

Force (Wedge Electrode)	Direction	Amplitude
Electric field force, F_q	$-\theta$ (q_z,V > 0) $+\theta$ (q_z,V < 0)	$F_q = 0.832\|q_{\pm}E_{r\theta}\|$(d = 0) $F_q = 0.832\|q_{\pm}E_{r\theta}\|$(d ≠ 0)
Electric field gradient force, F_{grad}	$-r$	$F_{grad} = 2\pi r^3\varepsilon_0\varepsilon_s\left\|\nabla {E_{r\theta}}^2\right\|$
Viscosity, F_v	Opposite the direction of movement	$F_v = 6\pi\rho_s rv$
Gravity, F_g	$-z$	$F_g = (4/3)\pi r^3 g(\rho_p - \rho_s)$

Note: q_z represents the particle charge when it is on the electrode; $q_{\pm}$ represents the particle charge when it lifts off from the electrode; $E_{r\theta}$ represents the electric field of a wedge-shaped electrode and θ is the angle of the two electrodes; r is the radius of the spherical conductive particle, mm; v is the velocity of the particle; g represents the gravitational acceleration; ρ_p is the particle density, kg/m^3; ρ_s is gas density, kg/m^3.

When the metal particles move, they are subjected to drag force exerted by the gas. The gas drag force F_d can be expressed as:

$$F_d = \frac{dy}{dt}\pi r\left(6\mu K_d\left(\frac{dy}{dt}\right) + 2.656\left(\mu\rho_s g l\frac{dy}{dt}\right)^{1/2}\right) \tag{10}$$

where μ is the viscous fluid coefficient (SF: 15.5 × 10^{-6} kg/m at 20 °C); r is the radius of the spherical conductive particle, mm; ρ_s is the gas density, kg/m^3; l is the particle length, mm; K_d is the gas drag force coefficient; and g is the gravity acceleration [39].

The following empirical formula can be used to determine the influence of gas pressure p on drag force ρ_g:

$$\rho_g = 7.118 + 6.332p + 0.303p^2 \tag{11}$$

where p is the gas pressure.

Based on the force analysis of metal particles and the parallel electrode model, H. Anis et al. calculated the floating voltage of spherical and linear particles while considering the effects of gravity and the electric field force, as shown in Equations (12) and (13) [33,40].

$$E_l = 473.8\sqrt{\frac{r\rho_s}{K}} \tag{12}$$

$$E_l = \left[\ln\left(\frac{2l}{r}\right) - 1\right]\sqrt{\frac{r^2\rho_s g}{\varepsilon l[\ln(l/r) - 0.5]}} \tag{13}$$

where r is the cross-sectional radius of wire conductive particles, mm; K is the correction coefficient, taken as 0.832 in this work; ρ_s is the gas density, kg/m^3; l is the particle length, mm; and ε is the dielectric constant.

Focusing on the slightly uneven electric field in GIS, Japan's Koh-ichi Sakai et al. proposed a wedge-shaped electric field model of metal particle movement. In the electric field, the critical field strength and the floating field intensity of the horizontal movement of spherical metal particles are obtained, accounting for the impact of the electric field gradient force E_H and the gas buoyancy E_L, as shown in Equations (14) and (15) [11,26].

$$E_H = \left\{\frac{2r\mu(\rho_p - \rho_s)(g - \beta)l_0}{\varepsilon_0\varepsilon_1[0.832\pi^2(r + \mu x_0 + 6r)]}\right\}^{1/2} \tag{14}$$

$$E_L = \left[\frac{2r(\rho_p - \rho_s)(g - \beta)l_0}{0.832\pi^2\varepsilon_0\varepsilon_1}\right]^{1/2} \tag{15}$$

where μ is gas viscosity coefficient; ρ_p is the particle density, kg/m^3; ρ_s is the gas density, kg/m^3; β is the buoyancy correction parameter; r is the radius of the spherical conductive particle, mm; l_0 is the distance between the edge of the wedge electrode and the origin of

the wedge electrode, that is, the extension line intersection, mm; x_0 is the distance between the particle and the edge of the wedge electrode, mm; ε_0 is the vacuum dielectric constant; and ε_1 is the relative dielectric constant of the gas.

Without considering the static friction at the metal particles' initial moment, when the metal particles move horizontally, the voltage U_L is calculated as [41,42]:

$$U_L = 165.9r\theta_0\sqrt{R_p(g-\beta)(\rho_p-\rho_s)\cos\theta_t} \tag{16}$$

Once certain conditions are met, the metal particles float, and the critical voltage U_H at this time is:

$$U_H = 475.6r\theta_0\sqrt{\frac{\mu R_p(g-\beta)(\rho_p-\rho_s)\left(\cos\theta_t+\frac{\sin\theta_t}{\mu}\right)}{6R_p+0.832\pi^2\mu r}} \tag{17}$$

In Equations (16) and (17), r is the radius of the spherical conductive particle, mm; θ_0 is the wedge electrode angle; R_p is the quality of particles; and θ_t is the angle between the direction of the electric field and the direction of gravity.

In a wedge-shaped electric field under DC voltage, metal particles are affected differently by the electric field gradient force at various positions. The initial voltage of the spherical metal particles, V_h, is obtained when its horizontal movement reaches a specific position. The following equation is used to calculate V_h while considering gas buoyancy and neglecting friction force [28]:

$$V_h = 165.9r\theta_0\left(\frac{r\mu\rho_p g}{1.731l+\mu x_0}\right)^{1/2} \tag{18}$$

When the floating condition is satisfied instead of the initial condition for horizontal movement, the metal particles float. The floating voltage, V_l, can be expressed as:

$$V_l = 165.9r\theta_0(l\rho_p g)^{1/2} \tag{19}$$

In Equations (18) and (19), μ is the gas viscosity coefficient; ρ_p is the particle density, kg/m^3; r is the radius of the spherical conductive particle, mm; l is the length of the wire particle, mm; θ_0 is the wedge electrode angle; x_0 is the distance between the particle and the edge of the wedge electrode, mm; and g is the gravity acceleration.

In the coaxial electrode, the floating voltage of linear metal particles, E_l, on the shell surface represents the particles [36,42]:

$$E_l = \sqrt{\frac{\rho_s g r}{1.43\varepsilon_0}} \tag{20}$$

where g is the gravity acceleration; ε_0 is the dielectric constant of the gas; r is the radius of the spherical conductive particle, mm; and ρ_s is the gas density, kg/m^3.

The floating field intensities of spherical and linear metal particles have been compared using different calculation models [20–22,43]. In Figure 5, the left diagram shows the changing strength of the floating field of spherical metal particles with different radii under four different models. The figure on the right shows the varying strength of the floating field of linear metal particles with different lengths under four different models.

The metal particle material also changes the floating field intensity. For copper metal particles, the floating field intensity increases significantly. Compared with aluminum, the floating field intensity of copper with the same length reaches 12 kV/cm (r = 0.12 mm); for copper with the same maximum radius, the stress reaches 25 kV/cm. Table 5 shows the critical floating field strength of metal particles.

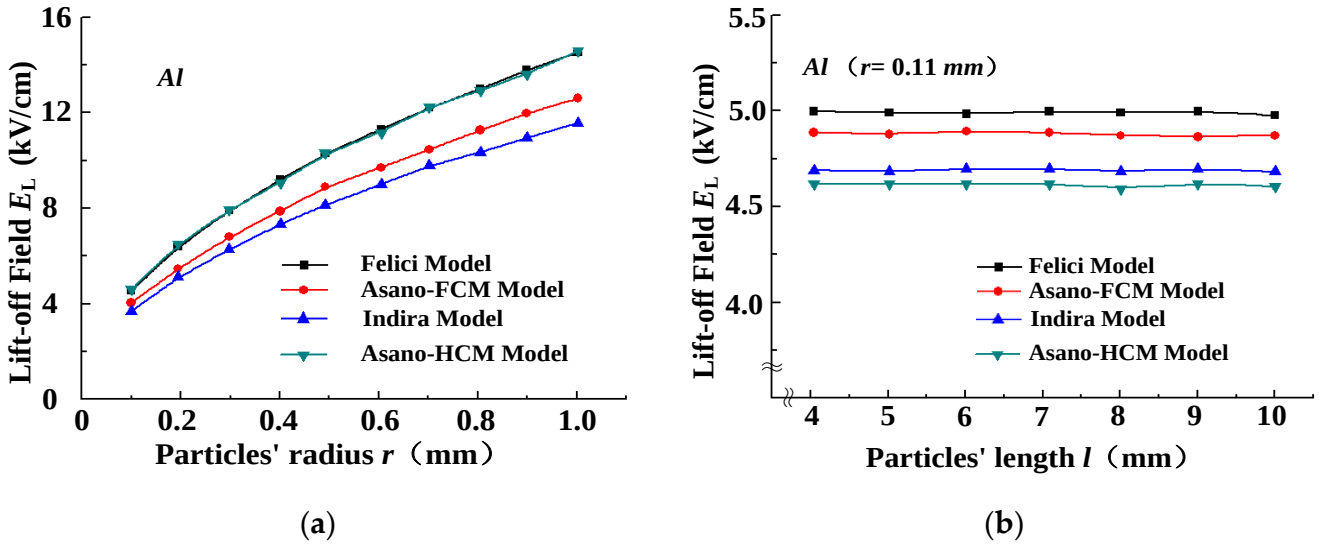

Figure 5. Floating field intensity of spherical and linear metal particles; (**a**) changing strength of the floating field of spherical metal particles (influenced by the particle radius); (**b**) changing strength of the floating field of spherical metal particles (influenced by the particle length).

Table 5. Critical floating field intensity of metal particles.

Characteristics	Sphere (Radius *r*)	Hemisphere (Radius *r*)	Semi-Ellipsoid (Radius *r*, and Length *l*)
Critical field strength	$0.49\frac{r\rho g}{\varepsilon}$	$0.27\frac{r\rho g}{\varepsilon}$	$\frac{0.82[\ln(\frac{l}{r})-1]r^2\rho g}{\varepsilon l\left[\ln(\frac{2l}{r})-\frac{1}{2}\right]}$
Characteristics	Linear particles (radius *r*, additionally, length *l*)	Half cylinder (radius *r*, and length *l*)	Thin foil (area *S* (small), and height *h*)

3.2. Movement of Metal Particles under DC Voltage

Whether metal particles move toward the high-voltage electrode and discharge is related to the ionization factor *K* [44]. When Equation (12) is satisfied, the metal particle will discharge. After discharge, the charge of the metal particles changes, and the force's movement varies accordingly:

$$\int_{\mathrm{d}} \overline{\alpha} dz \geq K \ (K = 10) \tag{21}$$

where $\overline{\alpha}$ is ionization factor, and *K* is a constant (*K* = 10 for air; *K* = 10.5 for SF_6). The metal particles discharge when the above conditions are met.

The metal particles are charged, float, and move to the high-voltage electrode under DC voltage. If there is no micro-discharge, the particles collide with the high-voltage electrode (*d* = 25 mm) and discharge. They then charge in reverse polarity and move back at a lower speed than before the collision [45].

Figure 6 shows that spherical metal particles with different radii gradually increase their flight heights with the extension of flight time under DC voltage. With increased voltage, the floating process differs between spherical and linear metal particles: spherical particles float directly, and linear metal particles usually float after rising [46–48]. This is because linear metal particles usually have various charges when placed flat and erect. Since the floating heights of metal particles under voltage are comparable, research shows that, for a coaxial electrode (r_i = 10 mm, and r_0 = 35 mm) under switching DC voltage,

spherical metal particles (r = 0.75 mm) and linear metal particles (Φ_1 mm × l_3 mm) have a similar floating height [49–51].

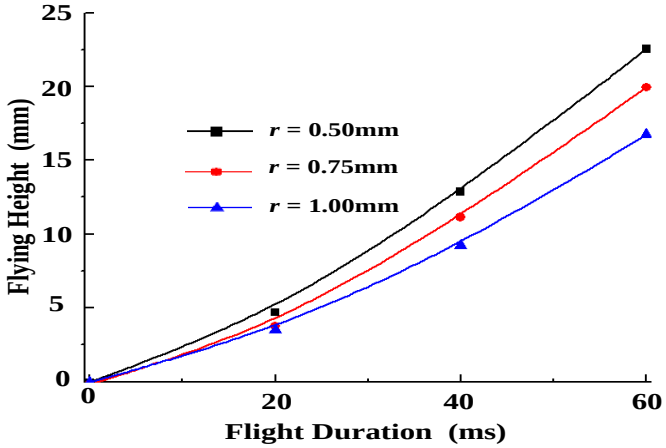

Figure 6. Variation in the flight height of spherical metal particles with different radii with increasing flight time.

3.3. Movement of Metal Particles under AC Voltage

The research on the movement of metal particles within electrodes includes their movement in space and their collision with the insulation or the electrode surface. The motion characteristics are primarily affected by the frequency and initial phase angle [30,46]. The electrode adopts a wedge shape under the following AC conditions: f = 60 Hz, and particle radius a = 0.5 mm. Spherical conductive particles based on AC voltage roll along the ground electrode surface to the high-field intensity area. Since the voltage polarity changes many times during movement between two collisions with the electrode, the direction of the electric field force experienced by the particles also changes multiple times, resulting in an uncertain direction of particle movement. In other words, the particles are characterized by a certain degree of randomness. Spherical conductive particles that move horizontally along the electrode surface always move in the direction of the stronger electric field. Its movement speed is related to the horizontal and the total electric field intensity distribution and intensity. The horizontal movement is affected by the horizontal and total electric field intensity distribution for linear conductive particles. Their vertical movement is subject to electric field intensity changes in the vertical direction.

In an AC electric field, it usually takes a relatively long time (100 ms) for the metal particles to float before the second jump occurs [30,45,46]. The movement of metal particles largely depends on the voltage frequency f and initial phase angle φ.

The minimum return position x_{min} and floating position x_{BD} of metal particles under the wedge electrode are influenced by the voltage frequency (0–500 Hz) [46] (see Figure 7). The trajectory of spherical conductive particles in an uneven electric field has the following two modes: the particles roll horizontally along the ground electrode surface, and the particles are lifted by the electric field force and make small "jumps" on the ground electrode surface, accompanied by horizontal directional and time-variable directional movement. When the voltage is constant, and $0 \leq f \leq 40$ Hz, the particles jump with penetrability and move to the high-field strength area; when $40 \leq f \leq 180$ Hz, x_{min} decreases as the frequency increases, and when $f > 180$ Hz, the particles do not collide with the high-voltage electrode and move in the direction of high field strength.

However, the trajectory of linear conductive particles in an uneven electric field has one mode: the particles float under the electric field force and make small "jumps" on the ground electrode surface, followed by horizontal and time-variable directional movement. This is because the friction on the particle is greater than the horizontal component of the electric field force when the particle is on the electrode surface.

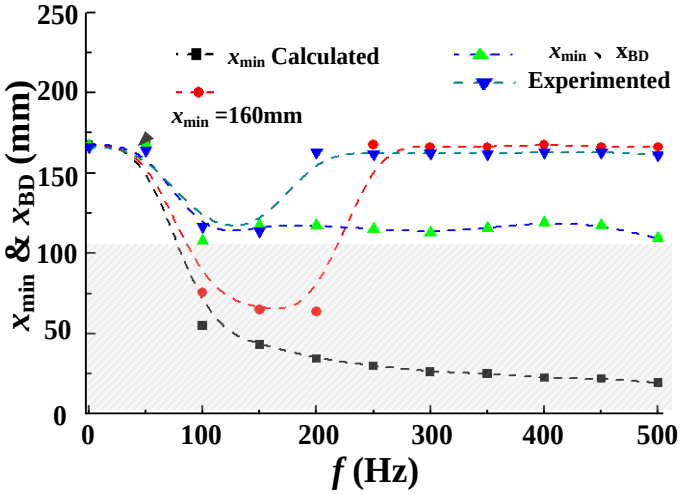

Figure 7. Relationship between the smallest takeoff position and voltage frequency under the wedge electrode (r = 0.5 mm; V_{peak} = 14.1 kV; φ_0 = 90°; 0.1 MPa pressure).

3.4. Movement of Metal Particles under the Superimposed Electric Field

3.4.1. Movement Characteristics of Particles on the Surface of a Bare Electrode

The floating height of metal particles has a higher amplitude (coaxial electrode 40/137) under AC and impulse voltage. At this time, the height of the alternating current (200 kV) is 9.7 mm, and that of superimposed lightning impulse voltage (1050 kV) is 55.2 mm. Figure 8 shows the movement characteristics of metal particles under AC and superimposed impulse voltage [47–49].

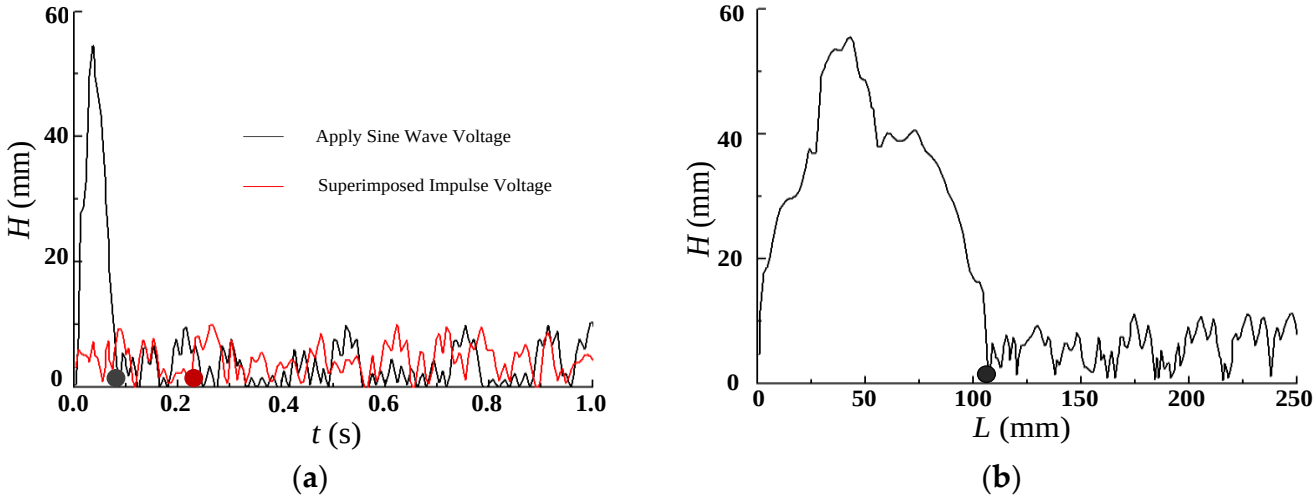

Figure 8. Particle motion in the coaxial electric field under AC and impulse voltage (in 137 mm/40 mm enclosure for *Al* particle with 75 kV/10 mm/0.25 mm radius); (**a**) particle motion in a coaxial electric field under AC voltage; (**b**) particle motion in a coaxial electric field under impulse voltage.

3.4.2. Movement Characteristics of Particles on the Coated Electrode Surface

Under AC voltage, the particle lifting voltage is significantly increased with coated electrodes. Under the same conditions, the lifting voltage of silicone rubber coating is higher than that of polyethylene terephthalate (PET). Moreover, the lifting voltage after the coating is 1–2 times that of the bare electrode. The particle lifting voltage increases to a greater extent under AC voltage compared with DC voltage. Figure 9 compares the lifting voltage of parallel plate electrodes coated with PET film and electrodes coated with silicone

rubber film. The red line is the change curve of the lift voltage when the PET film is the coating, and the black line is the curve when the rubber film is the coating [28,50,51].

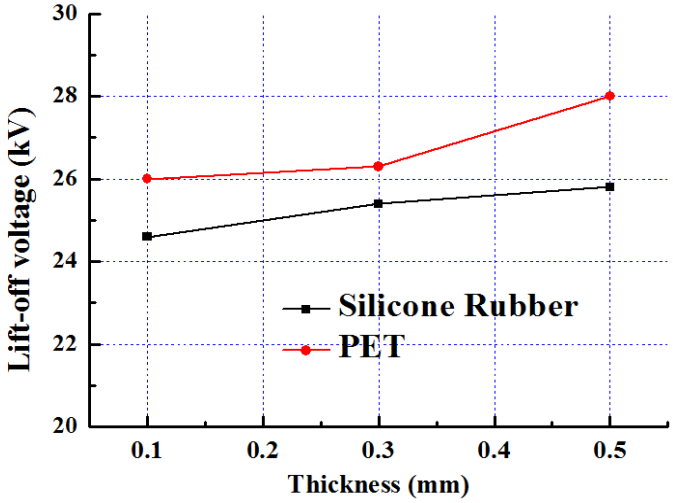

Figure 9. Relationship between particle lift-off voltage and thickness of silicone rubber and PET coatings.

When the lightning voltage is superimposed on the surface of the shell of the power frequency voltage, the metal particles with the coated electrode are affected by the lightning pulse as the applied voltage increases. Its maximum radial motion increases and is larger on the coated electrode surface than the bare one. As the thickness of the film increases, the maximum value decreases. Table 6 shows the radial motion of Cu particles [39].

Table 6. Radial motion of Cu particles on the bare electrode surface and coated surface.

Voltage (kV)	Maximum Radial Motion (mm)		
	Bare Electrode	Coating (50 μm)	Coating (100 μm)
100	3.66	0.0130	0.0120
132	10.08	0.0137	0.0716
145	12.19	0.2161	0.1379

Compared with the coated electrode system, movement in the uncoated electrode system is significantly greater. When the coating thickness increases, the particle charge decreases, and the maximum scale of movement decreases. Figure 10 shows the motion model of the coated bus's superimposed lightning impulse.

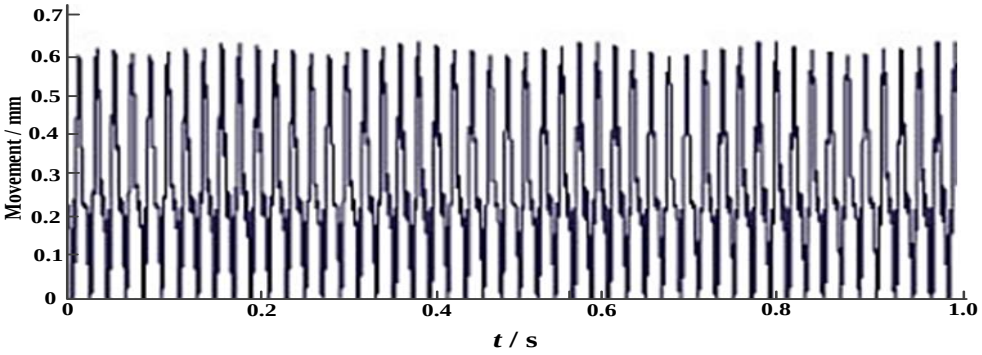

Figure 10. Movement pattern with the superimposed lightning impulse (908) for the coated enclosure AG/100 kV/10 mm/0.25 mm radius.

The coated electrode does not affect the final particle charge but prolongs the charging time compared with the bare electrode.

Interfacial polarization refers to the process of electrode surface charge transfer to the medium and gas interface. The particles on the coated electrode are subjected to the Coulomb force and electrostatic adsorption force [27].

The Coulomb force F_c is:

$$F_c = F_0\left(1 - e^{-\frac{t}{\tau}}\right) \tag{22}$$

where F_0 is the Coulomb force exerted by particles on the bare electrode, τ is the time-varying characteristic of the particle charging current, and t is the particle charging time.

The electrostatic adsorption force F_a is:

$$F_a = \frac{1}{2k_1}\left(1 - \frac{1}{\varepsilon_2}\right)F_c \tag{23}$$

where k_1 is the correction coefficient caused by the surface charge, and $k_1 = 0.832$.

Figure 11 shows the Coulomb force and electrostatic adsorption force on the particles when $\varepsilon_2 = 3.8$; the black line is F_c, and the red line is F_a. They increase because the charge on the particle increases with time.

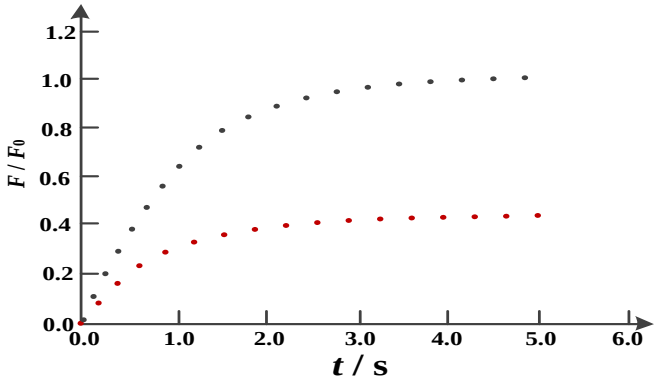

Figure 11. Time-varying electrostatic adsorption force on the particles.

In the charging process of particles with the coated electrode, the Coulomb force and electrostatic adsorption force gradually increase. Under this condition, even if the applied voltage reaches the movement's lifting voltage, the particles experience a time lag instead of moving immediately.

During lifting, the particles move vertically upwards and collide with the upper plate. After the collision, they move with acceleration toward the downward plate, and their electric charge becomes positive. However, instead of changing the electrical properties, the particle charging time reduces the charge during the short collision process. Consequently, the decrease causes the particles to bounce and accelerate their downward movement once more. In addition, the inelastic collision between the particles and the insulating film leads to a momentum loss, and as a result, the particles cannot reach the height of the upper electrode plate when flying away from the insulating film. The particles continuously collide with the film of the lower plate and bounce until they are stationary, continuously reducing their bounce height. This damped oscillation frequency is lower than the persistent oscillation frequency of the bare electrode. Once the particles are stationary on the insulating film, a certain amount of time is required to charge for "re-lifting".

Figure 12 shows the phenomenon of the continuous, intermittent lifting of particles [27,28] on the electrode surface coated with PET.

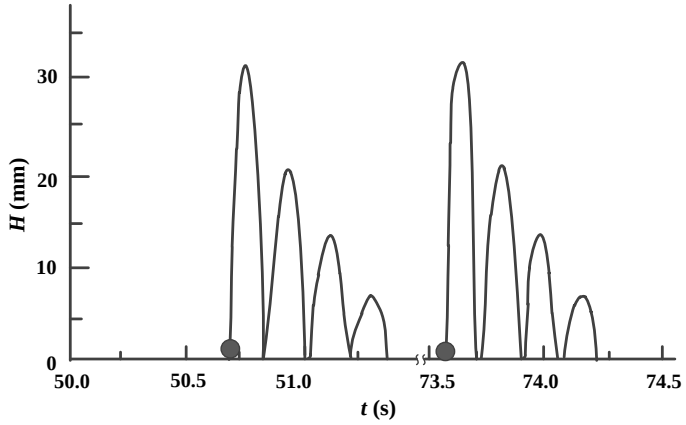

Figure 12. Lifting of the coating particle.

The particle re-lifting time is significantly shorter than the delay of the first particle charge because the particles collide with the film many times when they have a damped oscillation. Their positive charge is significantly reduced, or the particles acquire a certain amount of negative charge. Therefore, the recharging time is greatly shortened. The voltage affects the charging speed so that the re-lifting time decreases as the voltage increases (see Figure 13) [27].

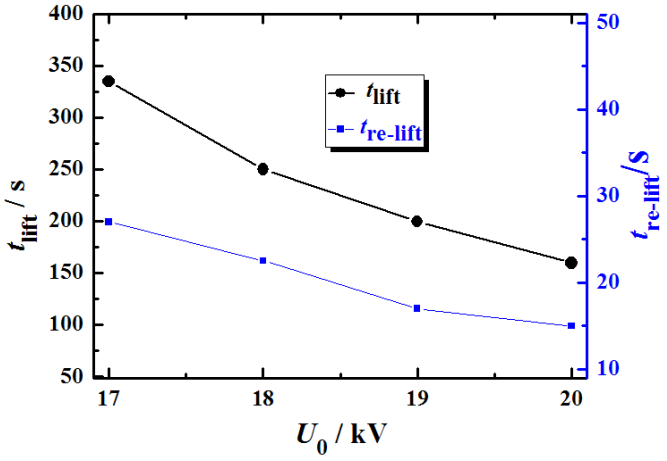

Figure 13. Comparison of lifting and re-lifting times of metal particles under different voltages.

3.5. Current Shortcomings and Prospects

Metal particle charging and movement have been studied for more than 20 years. The uniform electric field and the slightly uneven charged movement of metal particles have been extensively researched.

However, this research area has the following practical shortcomings:

- The metal particle charge in an uneven electric field. The electrification of metal particles in a uniform electric field can be analyzed according to N. N. Lebedev's model. However, whether the particles are charged according to this rule in an uneven electric field remains unclear. There is a considerable gap between the calculated electrification and the actual measurement.
- The charging process of metal particles. Although the metal particle charge can be calculated, the response to the transient process has yet to be analyzed, resulting in uncertainty in the metal particle movement when affected by overvoltage.
- The impact of the electric field on metal particle discharge. Research on calculating metal particle discharge and residual charge near different electrodes is not compre-

hensive. As a result, there is an urgent need to conduct such studies since conclusions are lacking.

Subsequent work will analyze the metal particle charging and discharging process (charge transfer process) to understand the mechanism of electric field and voltage effects on the movement of metal particles.

4. Movement of Conductive Particles near the Insulating Support

4.1. Movement of Conductive Particles near the Uncoated Electrode Insulator

A polypropylene insulating support structure was used to observe the movement of metal particles near the insulating support between wedge-shaped electrodes, wherein the electrode radius R was 160 mm, the center height was 10 mm, and the DC test voltage was 0–15 kV. The metal particles were in the form of stainless steel balls (r = 0.5 mm) and aluminum linear particles (diameter D = 0.25 or 0.5 mm and length l = 2–3 mm) [21]. The results showed that the metal particle movement was significantly different from that without an insulator when the particles were 4 mm from the insulator support under experimental conditions. Under an electric field force, the particles moved toward the high-voltage electrode.

Additionally, the results showed that insulators reduced the initial movement voltage of the metal particles [19]. The insulator type is shown in Figure 14. When the particle was near T-type and C1-type insulators, its initial movement voltage decreased by less than 10% compared with that without an insulator. R-type insulators reduced the initial movement voltage of the metal particles. The initial voltage near T-type and C1-type insulators decreased by less than 10% compared with that without an insulator. At a distance of x_0 = 2 mm from the R-type insulator, it was reduced by 27% compared with that without the insulator.

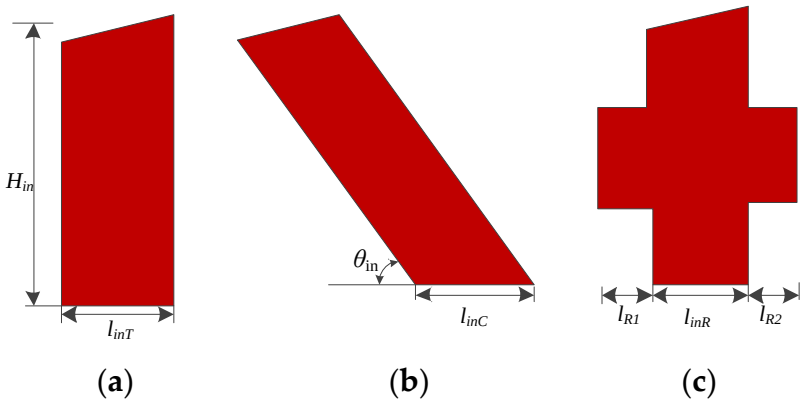

Figure 14. Tested spacer configuration: (**a**) T-type, (**b**) C1-type, (**c**) R-type.

The movement of metal particles near a polytetrafluoroethylene (PTFE) insulator has similar characteristics to those described in references [19,26]: the particles move horizontally and then float, float directly, or move horizontally until they adhere to the surface of the insulator. Furthermore, the range of insulator influence on particle movement is related to the insulator shape. Specifically, the spatial distortion of the electric field caused by the insulator is the main reason for the change in the particle trajectory. The particles in the distorted electric field can quickly move toward the insulator.

Under AC voltage (a = 0.5 mm, l = 2 mm, and D = 0.15 mm in a slightly uneven electric field below 10 kV), the embedded electrode arrangement can improve the electric field distribution near the insulator and prevent free conductive particles from adhering to its surface. It also increases the voltage required for particle floating near the insulator and suppresses particle floating [30].

K. Sakai et al. similarly adopted a wedge-shaped electrode test device supported by a PTFE pot insulator to explore particle movement characteristics. The results show that

the areas of particle movement can be divided into four zones (see Figure 15). In zone A, the particles move toward high-field strength areas. The particles in zones B and C move toward the insulator under DC voltage and adhere to the insulator surface after the collision. However, under AC voltage, the particles in zones B and C change their movement direction and no longer contact the insulator after the collision. The particles in zone D also move toward high-field intensity zones.

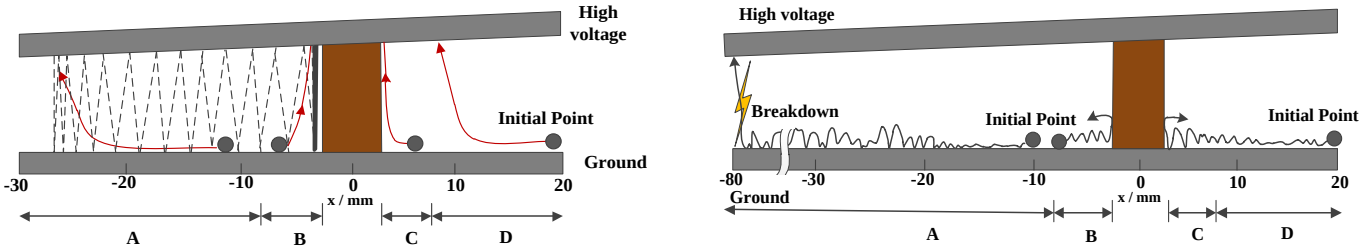

Figure 15. Trajectory of a spherical particle around the T-shaped insulator: (**a**) under DC voltage; (**b**) under 60 Hz AC voltage.

4.2. The Influence of Coating on Particle Movement

Li et al. used PET coating on the ground electrode to explore particle movement characteristics under DC voltage [27]. The results showed that the particle lifting field intensity increased due to the changed particle charge (the maximum charge was at the contact between the particles and the film). The particles' rising height around the insulator was significantly reduced as the charge weakened, and the electric field direction changed. However, Wang et al. hypothesized that the coating method only changes the particle charging time under DC voltage and that the total charge does not change. Specifically, the lifting field strength of particles is improved by electrostatic adsorption to the coating, and the charge time causes the "intermittent lifting" of particles around the insulator.

Zhang et al. built a 300 kV GIS test device and used a coating layer made of epoxy resin to explore the particle movement characteristics under the coating layer condition. The results showed that, regardless of the applied voltage waveform, polarity, and frequency, the enhancing effect of the lifting field strength of particles caused by the dielectric coating was more active under AC voltage than under DC voltage. In their subsequent study [28], they observed that particles did not move under standard or even high DC voltage. The particles could only "reciprocate" under positive DC voltage with oscillation. Moreover, the larger the particle size, the longer the particle "reciprocation" time. A similar experiment is reported in Ref. [51], but the coating layer consisted of a high-conductivity material. The coating made the electrode surface smoother and reduced the pre-breakdown current in the air gap. Therefore, it decreased the charge and rising height of the particles.

K. Sakai et al. discussed the coating's influence on particle movement when studying a method of particle suppression. They used a round convex electrode. The angle between the convex electrode and the plane was 3.5 degrees, and the coating material was polytetrafluoroethylene (see Figure 16). When not coated, the particles moved to the insulator and were eventually adsorbed on its wall or fell into a trap and deactivated. However, the particles occasionally adhered directly under the insulator walls. As the voltage increased, these particles escaped from the insulator and reached the high-voltage electrode. Then, they oscillated back and forth between poles. After coating the ground electrode with a PET layer, the particles only moved in the horizontal direction due to the increased lifting field strength. After contacting the insulator, these particles climbed up the insulator because of their changed charge. As a result, they fell into the insulator wall and became inactivated without moving to the high-voltage pole.

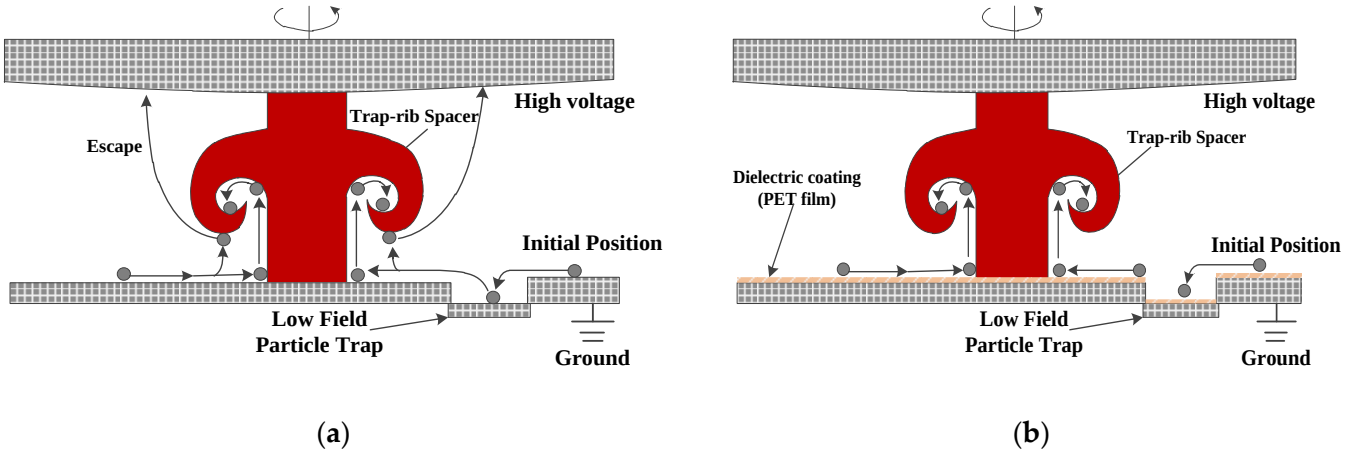

Figure 16. Particle motion around the insulator: (**a**) no PET film was applied; (**b**) PET film was applied.

4.3. Current Shortcomings and Prospects

A slightly uneven electric field analysis model has been established based on calculating the charged metal particles in a uniform electric field. The obtained results are the floating and collision characteristics and movement changes of metal particles near the insulation, with or without insulation support. However, there are still the following shortcomings in analyzing metal particle movement:

- Although models of the uniform electric field, slightly uneven wedge electric field, and coaxial electrode electric field have been built, the analysis of the electric field gradient force on metal particles in each model lacks an individual correspondence, leading to significant errors in research conclusions.
- The models lack the ability to quantitatively analyze the influence of the insulation mechanism on metal particles, though four insulating support models have been established, and the metal particle movement has been analyzed using each one. Due to this shortcoming, it is difficult to guide the practical design of the electric field and insulation.

Subsequent work should focus on the final stable motion state of metal particles, including their resonance motion and the adhesion criterion on insulating surfaces.

5. Discharge Characteristics of Conductive Particles on the Insulating Surface

Conductive particles attached to the insulating surface can cause a surge in surface charge accumulation [52–58]. The conductive particles attached to the middle position induce a substantial increase in the charge. However, suspended particles have little effect on the surface charge accumulation. Research has found that when the vertical distance from the suspended particles to the insulator surface exceeds four times the particle diameter, the impact on the insulator surface charge can be neglected [10,12,55,56]. The charges accumulated on the insulating surface also produce a Coulomb effect on the conductive particles and modify the electrical field gradient force that they experience, thus changing their discharge characteristics.

5.1. Charging Behavior of Conductive Particles on Insulating/Coated Surfaces

Studies have shown that multiple factors alter the charging behavior of conductive particles on the insulating surface. From a quantitative perspective, researchers around the world have always assumed that the particle shape does not affect the particle mechanism or force types and often study spherical particles [46,47]. To find the source of metal particle charging in a uniform DC field, researchers have studied the charging of metal particles when they are stationary on the electrode surface [16,27]. They used the potential function

caused by multi-pole expansion to solve the partial differential equations in the electrostatic field zones and obtained the spherical metal particle charge q_b:

$$q_b = \oint_s Dds = \frac{2}{3}\pi^3 \varepsilon_0 \varepsilon_1 r^2 E_0 \quad (24)$$

where D is the electric flux density; ε_0 is the vacuum permittivity; ε_1 is the relative dielectric constant of the gas between the electrodes; r is the radius of the spherical conductive particle, mm; and E_0 is the electric field intensity, kV/cm.

Li et al. studied linear conductive particle charging. The charge is related to the particle position and shape [25,27], and the charges of particles positioned vertically and horizontally on the electrode surface are derived from this relationship, respectively. After being charged, the metal particles move because of the electric field force.

Coating the insulating surface improves some of its properties, such as surface roughness. The surface-coated insulator has an enhanced surface electric field distribution and decreased surface charge accumulation, increasing the flashover voltage along the insulator surface. From another perspective, when colliding with the coated insulating film, the conductive particles become charged. The obtained charge is significantly less than that of particles colliding with the bare electrode, thereby reducing the movement activity. This may be related to the time effect of the charge accumulation on the insulating film's surface. In Ref. [27], the conductive particle charge was measured using the Faraday cup method (see Table 7), which demonstrated that particle charge decreased when it lifted off from the filmed surface.

Table 7. Particle charge measured by the Faraday cup method.

Voltage Type	x_0/mm	V_h/kV	q_{film}/pC (Measured Value)	q_{bare}/pC (Calculated Value)
DC	95	8.8	−98	−215
	130	14.0	−134	−340
	180	20.2	−24.7	−505
AC	90	8.2	102	205
	115	12.4	−174	310
	145	16.4	−148	410

Table 7 shows that the conductive particle charge is about 30–60% under DC voltage when the insulation is not coated. Additionally, the charge polarity is the opposite of that of the applied voltage. Under AC voltage, the charge dispersibility of the conductive particles is greater, and their polarity can be positive or negative.

5.2. Movement Characteristics of Conductive Particles on Insulating/Coated Surfaces

Research has found that conductive particles are lifted under the electric field gradient force and radial Coulomb force. Due to the electric field distortion caused by the charge accumulation on the surface and the insulator, the conductive particles may be subjected to the axial Coulomb force and the electric field gradient force. As a result, the particles move toward the insulator and may eventually reach the surface. However, if there are defects on the insulator surface, particles may adhere to it or gather at the junction of the insulator and the electrode. The two ends of the metal particles attached or fixed to the insulator surface generate partial discharge, which intensifies the charge accumulation on the surface to affect the electric field distribution near the insulator (see Figure 17) [27].

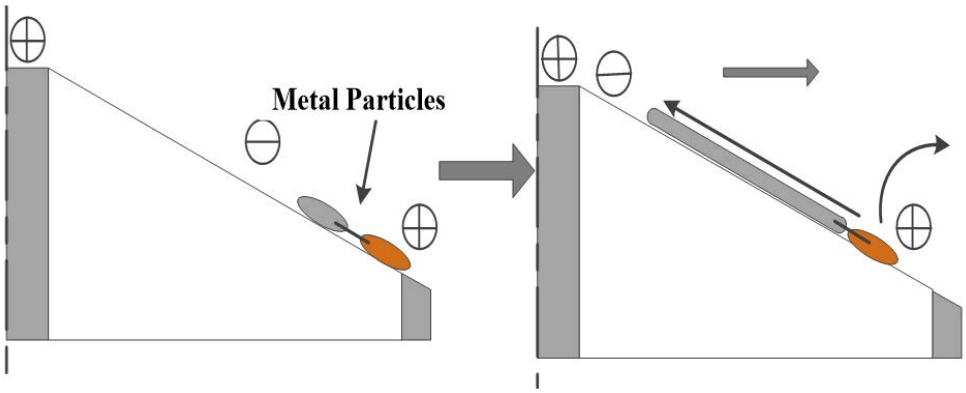

Figure 17. Trajectories of metal particles on insulating surfaces.

The movement behavior of conductive particles is the leading factor altering the insulation strength of GIS/GILs, and the movement characteristics are related to the applied voltage type. Studies have shown that in a DC GIL, the particle movement activity becomes more energetic due to the unipolar electric field force. Therefore, the particles can penetrate the electrode gap when they are lifted. The studies also report that the gas pressure, voltage polarity, and particle length do not affect the electric field intensity required for lifting. In addition, the conductive particles jump vigorously under the impulse voltage and penetrate the electrode gap [10,26]. The voltage required for particles to lift off or to penetrate the electrode gap is higher under impulse voltage than under AC or DC. Specifically, this involves linear particles accompanied by hovers and jumps of corona discharge near the negative electrode [49].

Many scholars around the world have studied the movement characteristics of conductive particles on an insulating surface. Their findings indicate that the particle movement characteristics are related to the initial particle position, voltage type, voltage amplitude, and reflection coefficient. Conductive particles with various initial positions have diverse trajectories under the same voltage. In the same condition, the particle trajectories change when step voltages with different amplitudes are applied (see Figure 18).

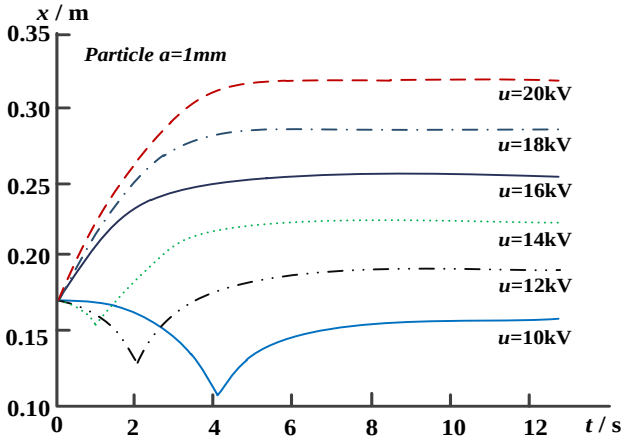

Figure 18. Relationship between particle trajectory and voltage amplitude.

When reciprocating in the electrode gap, the conductive particles collide with the electrode and reflect. The tangential reflection coefficient γ_1 and normal reflection coefficient γ_n are usually used to express the relationship between particle incident and reflection velocities. Figure 19 shows the particle trajectories with different reflection coefficients.

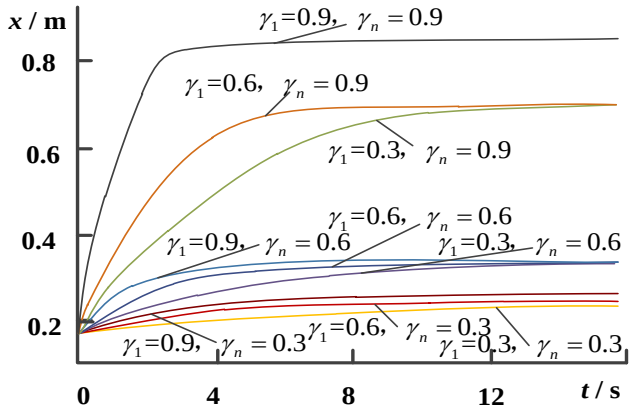

Figure 19. Particle trajectories with different reflection coefficients.

In addition, γ_n affects the position at which the particle finally resonates, and γ_1 changes the time required for the particle to reach resonance.

5.3. Influence of Conductive Particles on Discharge Characteristics

Conductive particles move with the electric field force in GIS/GILs, which can cause breakdown between the electrodes or induce flashover along the insulator. Studies have shown that conductive particles reduce the gas insulation performance between electrodes. The comparison shows that the gas insulation strength decreases significantly as the conductive particle length increases and the particle diameter decreases (see Figure 20a). Under AC conditions, when the conductive particles in the coaxial electrode (76/254, bare electrodes) increase to 6.5 mm, the insulation strength is reduced by 35% compared with that with no particles (see Figure 20b) [17,22,23,57].

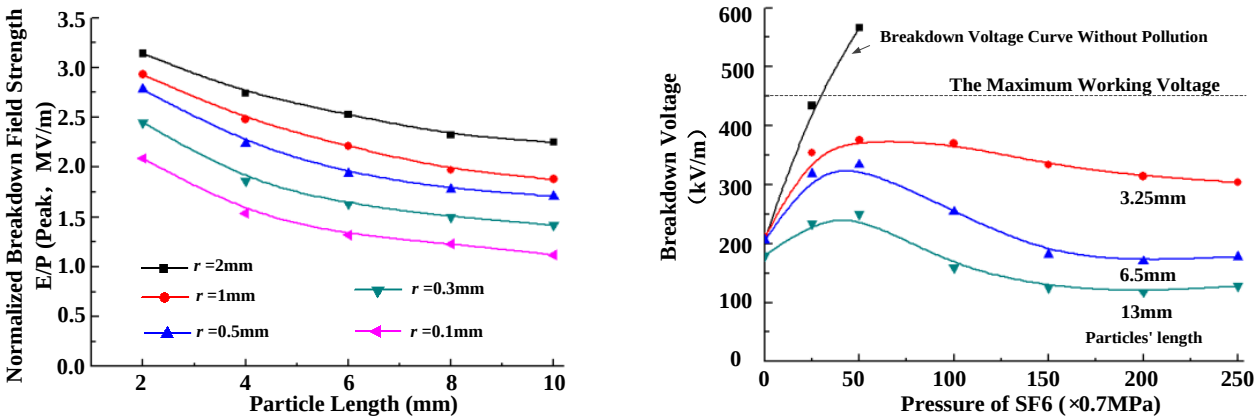

(**a**) (**b**)

Figure 20. Effect of linear particles of different sizes on gas electric field intensity and breakdown voltage between electrodes; (**a**) relationship between linear particle size and gas electric field intensity; (**b**) relationship between linear particle size and breakdown voltage between electrodes.

When metal particles are attached to the insulator surface, their impact on the insulator's flashover voltage is related to the particle length and distribution on the insulator. The flashover voltage drops by about 25% when the particles in the middle of the supporting insulator increase from 3 to 6 mm. Since the metal particles studied by the free-spread method increase from 2 to 5 mm, the tangential electric field component is reduced by more than 30% during flashover [18,57,58].

In references [18,54], when conductive particles with a length of 2.3 mm were attached to the insulator surface, the field strength in the vicinity increased to about 1.2 times the original field strength. However, when conductive particles of the same size adhered to the insulator surface, they had a more significant impact on the field strength, increasing it to 3.4 times the original strength. Furthermore, the study found that the particle position also changed the electric field distribution: the degree of the surface electric field distortion decreased as the electrode distance increased.

6. Conclusions and Prospects

The coating material applied to the electrode and insulator influences particle charging characteristics, movement, and discharge. Particle charging, movement, and charge transfer in DC, AC, and superimposed electric fields were compared between different surfaces, and several conclusions are summarized as follows:

- The charge of metal particles on the bare electrode surface is mainly due to induced charges and is proportional to the applied electric field. The particle can be charged instantaneously. The charge of metal particles on the coated electrode surface is mainly affected by conduction. When the applied electric field passes a certain threshold, the metal particle charge markedly increases and accumulates as time increases. The time effects on the charge of insulating coating surface particles have not been researched. Research trends suggest that future studies will focus on the relation between the surface charge and spatially charged conductive particles.
- When the electrode is bare, the same field strength is needed for the floating of metallic particles in AC and DC electric fields. When the electrode is coated, the field strength needed for metallic particles to float is higher in the DC electric field than in the AC electric field. The metallic particle oscillates between electrodes in the DC electric field, preferring to move toward higher electric field strength. In the AC electric field, the metallic particle jumps on the electrode surface with a small distance, and the distance decreases as the power frequency increases, which increases the chance of collision between the metallic particle and the electrode. In the DC electric field with a coated electrode, the metallic particle has interval and single directional movement. It is easier to recognize metallic particle defects. Therefore, future research can focus on effective methodologies for the detection of metallic particle defects by applying a combination of pulsing, DC, and AC electric fields.
- When the bare electrode is used in a DC electric field, the metal particle oscillates along the insulator surface near the insulating support, and flashover readily occurs. In the AC electric field, the distance of metallic particle movement around the insulator increases. When the electrode is coated, the distance of metallic particle movement decreases, and the metallic particle motion becomes predictable and controllable. Furthermore, when the electrode is coated, it increases the activation potential of metallic particles, reducing the chance that it will be lost. Investigating the functionalities of innovative coating materials, together with insulator dielectric properties and metallic particle trapping designs, is a promising research direction.

Author Contributions: Conceptualization, J.S.; methodology, S.S.; software, S.S. and X.L.; validation, F.D. and J.R.; formal analysis, J.S. and S.S.; investigation, J.S., S.S. and Y.L.; resources, C.G.; data curation, S.S.; writing—original draft preparation, J.S. and S.S.; writing—review and editing, J.S., Y.L. and S.S.; visualization, S.S.; supervision, J.S.; project administration, S.S. and J.R.; funding acquisition, J.S. and X.L. All authors have read and agreed to the published version of the manuscript.

Funding: This research was funded by Fundamental Research Funds for the Central Universities (2021JBM025) and National Natural Science Foundation of China (51907003).

Institutional Review Board Statement: This study did not involve humans or animals.

Informed Consent Statement: Informed consent was obtained from all subjects involved in the study.

Data Availability Statement: This study did not report any MDPI Research Data.

Acknowledgments: This work was supported by the Fundamental Research Funds for the Central Universities (2021JBM025), National Natural Science Foundation of China (51907003), Fundamental Research Funds for the Central Universities (E18JB00070, E17JB00020), and Science and Technology Foundation of State Grid Corporation of China (B342GY160015).

Conflicts of Interest: The authors declare no conflict of interest.

References

1. Wang, F.; Fang, Z.; Qiu, Y. Study of charge accumulation on insulator surface in HVDC Gas-insulated switchgear. *Chin. J. Electr. Eng.* **2005**, *25*, 105–109. (In Chinese)
2. Li, C.; Lin, C.; Yang, Y.; Zhang, B.; Liu, W.; Li, Q.; Hu, J.; He, S.; Liu, X.; He, J. Novel HVDC spacers by adaptively controlling surface charges—Part II: Experiment. *IEEE Trans. Dielectr. Electr. Insul.* **2018**, *25*, 1248–1258.
3. Christodoulou, C.A.; Vita, V.; Mladenov, V.; Ekonomou, L. On the computation of the voltage distribution along the non-linear resistor of gapless metal oxide surge arresters. *Energies* **2018**, *11*, 3046. [CrossRef]
4. Inoue, N.; Sato, S.; Yoshida, T.; Oida, Y.; Kumada, A.; Hidaka, K. Insulation properties of highly pressurized dry air-effects of anodic oxide coating and surface roughness of electrodes on breakdown voltage. *IEEE Trans. Dielectr. Electr. Insul.* **2014**, *21*, 2081–2087. [CrossRef]
5. Meijer, S.; Smit, J.J.; Gulski, E.; Girodet, A. Partial discharge early warning system in gas-insulated switchgear. In Proceedings of the IEEE/PES Transmission and Distribution Conference and Exhibition, Yokohama, Japan, 6–10 October 2002; 2002; pp. 931–936.
6. Ziomek, W.; Kuffel, E. Activity of Moving Metallic Particles in Prebreakdown State in GIS. *IEEE Trans. Dielectr. Electr. Insul.* **1997**, *4*, 39–43.
7. Li, C.; Zhu, Y.; Hu, J. Charge cluster triggers unpredictable insulation surface flashover in pressurized SF6. *J. Phys. D* **2020**, *54*, 67–70. [CrossRef]
8. Budiman, F.N.; Khan, Y.; Al-Arainy, A.A. Estimation of particle initiated PD inception voltage around spacer in GIS. In Proceedings of the 4th International Conference on Power Engineering, Energy and Electrical Drives, Itanbul, Turkey, 14 May 2013; pp. 517–521.
9. Sakai, K.; Tsuru, S.; Abella, D.L. Conducting particle motion and particle-initiated breakdown in dc electric field between diverging conducting plates in atmospheric air. *IEEE Trans. Dielectr. Electr. Insul.* **1999**, *6*, 122–130. [CrossRef]
10. Vita, V.; Christodoulou, C.A. Comparison of ANN and finite element analysis simulation software for the calculation of the electric field around metal oxide surge arresters. *Electr. Power Syst. Res.* **2016**, *133*, 87–92. [CrossRef]
11. Tan, X.; Guo, H.; Zhang, Q. Ultrasonic characteristics and state recognition of moving metal particles in GIS under DC. *High Volt. Technol.* **2010**, *36*, 391–395. (In Chinese)
12. Li, C.; Lin, C.; Hu, J.; Liu, W.; Li, Q.; Zhang, B.; He, S.; Yang, Y.; Liu, F.; He, J. Novel HVDC Spacers by Adaptively Controlling Surface Charges—Part I: Charge Transport and Control Strategy. *IEEE Trans. Dielectr. Electr. Insul.* **2018**, *25*, 1238–1247.
13. Wang, J.; Li, Q.; Li, B. Motion analysis of spherical conducting particle in DC GIL considering the influence of inelastic random collisions and SF6/N2 gaseous mixture. *Proc. CSEE* **2015**, *35*, 3971–3978. (In Chinese)
14. Li, C.; Hu, J.; Lin, C. The potentially neglected culprit of DC surface flashover: Electron migration under temperature gradients. *Sci. Rep.* **2017**, *7*, 3271. [CrossRef]
15. Zhang, L.; Lin, C.; Li, C. Gas–Solid interface charge characterisation techniques for HVDC GIS/GIL insulators. *High Volt.* **2020**, *5*, 95–109. [CrossRef]
16. El Bahy, M.M.; Ward, S.A.; Morsi, R.; Badawi, M. Particle-initiated breakdown in gas-insulated co-axial configuration. In Proceedings of the 2011 Annual Report Conference on Electrical Insulation and Dielectric Phenomena, Cancun, Mexico, 20 October 2011; pp. 722–727.
17. Murooka, Y.; Koyama, S. Nanosecond surface discharge study by using dust figure techniques. *J. Appl. Phys.* **1973**, *44*, 1576–1580. [CrossRef]
18. Iwabuchi, H.; Matsuoka, S.; Kumada, A.; Hidaka, K.; Hoshina, Y.; Yasuoka, T.; Takei, M. Influence of tiny metal particles on charge accumulation phenomena of GIS model spacer in high-pressure SF6 gas. *IEEE Trans. Dielectr. Electr. Insul.* **2013**, *20*, 1895–1901.
19. Jia, J.; Zhang, Q.; Shi, X. Motion of conducting particle near PTFE spacer under AC voltage. *Trans. Chin. Electrotech. Soc.* **2008**, *23*, 7–11.
20. Sun, J.; Zhi, Q.; Cui, B.; Bian, K.; Chen, W.; Yan, X. Particle trajectories and its charging behaviors: Effect of gas type and electric field. *Nanotechnology* **2021**, *32*, 105702. [CrossRef] [PubMed]
21. Sun, J.; Chen, W.; Li, Z.; Yan, X.; Cui, B.; Wang, H. Research on Experiment and Simulation of Charged Metal Particle Collision Characteristic. *IEEE Trans. Dielectr. Electr. Insul.* **2016**, *23*, 3117–3125. [CrossRef]
22. Sun, J.; Chen, W.; Bian, K.; Li, Z.; Yan, X.; Xu, Y. Movement Characteristics of Ball Metallic Particle between Ball-Plane Electrodes under DC Voltage. *IEEE Trans. Dielectr. Electr. Insul.* **2018**, *25*, 1047–1055. [CrossRef]
23. Levedev, N.N.; Skal'skaya, I.P. Force Acting on a Conducting Sphere in the Field of a Parallel Plane Condenser. *Sov. Phys. Tech. Phys.* **1962**, *7*, 268–270.
24. Pérez, A.T. Charge and force on a conducting sphere between two parallel electrodes. *J. Electrostat.* **2002**, *56*, 199–217. [CrossRef]
25. Sakai, K.; Abella, D.L.; Khan, Y. Experimental studies of free conducting wire particle behavior between nonparallel plane electrodes with AC voltages in air. *IEEE Trans. Dielectr. Electr. Insul.* **2003**, *10*, 418–424. [CrossRef]

26. Khan, Y.; Sakai, K.; Lee, E.K.; Suehiro, J.; Hara, M. Motion behavior and deactivation method of free-conducting particle around spacer between diverging conducting plates under DC voltage in atmospheric air. *IEEE Trans. Dielectr. Electr. Insul.* **2003**, *10*, 444–457. [CrossRef]
27. Wang, J.; Li, Q.; Li, B.; Liu, S.; Li, C. Mechanism analysis of the Electrode–Coating's Impact on the particle-lifting under DC voltage. *Trans. Chin. Electrotech. Soc.* **2015**, *30*, 119–127. (In Chinese)
28. Zhang, Q.; Jia, J.; Yang, L. Charging mechanism of metallic conducting particle on a dielectrically coated electrode in gas insulated system. *J. Xi'an Jiaotong Univ.* **2004**, *38*, 1287–1291. (In Chinese)
29. Intra, P.; Tippayawong, N. Development and evaluation of a Faraday cup electrometer for measuring and sampling atmospheric ions and charged aerosols. *Partic. Sci. Tech.* **2015**, *33*, 257–263. [CrossRef]
30. Sakai, K.I.; Abella, D.L.; Khan, Y.; Suehiro, J.; Hara, M. Theoretical and experimental studies for spherical free-conducting particle behavior between nonparallel plane electrodes with AC voltages in air. *IEEE Trans. Dielectr. Electr. Insul.* **2003**, *10*, 404–417. [CrossRef]
31. Runde, M.; Aurud, T.; Nokleby, J.E.; Skyberg, B.; Ljokelsoy, K.; Lundgaard, L.E. Risk assessment basis of moving particles in gas insulated substations. In Proceedings of the 1996 Transmission and Distribution Conference and Exposition, Los Angeles, CA, USA, 16 September 1996; pp. 181–188.
32. Lundgaard, L.E. Particles in GIS characterization from acoustic signatures. *IEEE Trans. Dielectr. Electr. Insul.* **2001**, *8*, 1064–1074. [CrossRef]
33. Zhou, K.; Boggs, S. Uniform Field Charge on a Conducting Particle. *IEEE Trans. Dielectr. Electr. Insul.* **2009**, *16*, 1158–1159. [CrossRef]
34. Ma, Y.; Cheng, Z.; Li, C. Experimental study of accelerating surface charge dissipation on polymer treated by repetitively pulsed discharge plasmas. *Proc. CSEE* **2016**, *36*, 731–1738. (In Chinese)
35. Kumada, A.; Okabe, S. Charge distribution measurement on a truncated cone spacer under DC voltage. *IEEE Trans. Dielectr. Electr. Insul.* **2004**, *11*, 929–938. [CrossRef]
36. Nojima, K.; Zhang, X.; Sato, M.; Yasuoka, T.; Shiiki, M.; Takei, M.; Boggs, S.A. Forces affecting metallic particle motion in GIS. In Proceedings of the 2014 International Symposium on Electrical Insulating Materials, Niigata, Japan, 5 June 2014; pp. 132–135.
37. Peng, Z.; Xie, H.; Fang, T. Effect of electrode surface coating on charge injection. *J. Xi'an Jiaotong Univ.* **1996**, *24*, 71–75.
38. Wang, J.; Li, B.; Li, Q.; Liu, S. Impact of Linear Metal Particle on Surface Charge Accumulation of Post Insulator within DC GIL. *Trans. Chin. Electrotech. Soc.* **2016**, *31*, 213–222.
39. Kumar, G.V.N.; Amarnath, J. Metallic particle dynamics in a single phase gas insulated busduct with coated electrodes under lightning impulse superimposed on power frequency voltage. *Eur. Trans. Electr. Power.* **2010**, *20*, 650–660. [CrossRef]
40. Anis, H.; Srivastava, K.D. Free Conducting Particles in Compressed Gas Insulation. *IEEE Trans. Dielectr. Electr. Insul.* **1981**, *16*, 4327–4338. [CrossRef]
41. Metwally, I.A.; A-Rahim, A.A. Dvnamic Analysis of Motion of Spherical Metallic Particles in Non-Uniform Electric Field. *IEEE Trans. Dielectr. Electr. Insul.* **2002**, *9*, 282–293. [CrossRef]
42. Jia, J.; Tao, F.; Yang, L. Motion analysis of spherical free conductive particles under non-uniform DC electric field in GIS. *Proc. CSEE* **2006**, *26*, 106–111. (In Chinese)
43. Felici, N.J. Forces ad charges of paticles in contact with a electrode under the influence of an electric feld. *Rev. Gener. L'Electr.* **1960**, *75*, 1145–1160.
44. Sakai, K.; Abella, D.L.; Suehiro, J. Mode of free-conducting particle motion and particle-triggered breakdown mechanism in non-uniform field gaps. In Proceedings of the 2000 Annual Report Conference on Electrical Insulation and Dielectric Phenomena (Cat. No.00CH37132), Victoria, BC, Canada, 15 October 2000; pp. 389–392.
45. Wang, J. Research on the Charged Motion Mechanism and Treatment Method of DC GIL Metal Particles. Ph.D. Thesis, North China Electric Power University, Beijing, China, 2017. (In Chinese).
46. Li, D.; Yang, J.; Liang, J. Characteristics of Acoustic Signal from Free Moving Metallic Particles in Gas Insulated Switchgear. *J. Xi'an Jiaotong Univ.* **2009**, *21*, 245–247. (In Chinese)
47. Farish, O.; Al-Bawy, I. Charge deposition and insulator flashover in SF6 under impulse voltages. In Proceedings of the IEE Colloquium on Charging and Tracking of Insulators in Gaseous and Vacuum Environments, London, UK, 8 May 1990; pp. 21–25.
48. Radwan, R.M.; Morsi, R.; Abd-Allah, M.A. Motion of free conducting particles in SF6 insulated systems under dc switching voltages. *IEEE Trans. Dielectr. Electr. Insul.* **1994**, *1*, 25–30. [CrossRef]
49. Zhang, Z.; Lu, F.; Liang, G. A High-Frequency Circuit Model of a Potential Transformer for the Very Fast Transient Simulation in GIS. *IEEE Trans. Power Deliv.* **2008**, *23*, 1995–1999.
50. Ansorge, S.; Schmuck, F.; Papailiou, K.O. Improved Silicone Rubbers for the Use as Housing Material in Composite Insulators. *IEEE Trans. Dielectr. Electr. Insul.* **2012**, *19*, 209–217. [CrossRef]
51. Al-Omari, A.N.; Lear, K.L. Dielectric characteristics of spin-coated dielectric films using on-wafer parallel-plate capacitors at microwave frequencies. *IEEE Trans. Dielectr. Electr. Insul.* **2005**, *12*, 1151–1161. [CrossRef]
52. Li, L.; Teng, L.; Huang, C. Envelope analysis and defects identification of Partial discharge UHF signals in GIS. *High Volt. Eng.* **2009**, *35*, 260–265.
53. Zuev, L.B.; Danilov, V.I.; Konovalov, S.V. Influence of contact potential difference and electric potential on the microhardness of metals. *Phys. Solid State* **2009**, *51*, 1137–1141. [CrossRef]

54. Li, C.; Hu, J.; Lin, C. The control mechanism of surface traps on surface charge behavior in alumina-filled epoxy composites. *J. Phys. D* **2016**, *49*, 33–36. [CrossRef]
55. Qi, B.; Li, C.; Hao, Z. Evolution phenomena and features of surface partial discharge initiated by immobilized metal particles on GIS insulators. *Proc. CSEE* **2011**, *31*, 101–108. (In Chinese)
56. Zou, Y.; Tang, Z.; Yan, W.; Yin, H.; Tang, C. Effect of Metallic Particles in DC GIL on Surface Charge Accumulation of Insulators. *Insul. Surge Arrester* **2020**, *22*, 236–243.
57. Li, C.; Hu, J.; Lin, C. Surface charge migration and dc surface flashover of surface-modified epoxy-based insulators. *J. Phys. D* **2017**, *50*, 20–25. [CrossRef]
58. Volpov, E. HVDC gas insulated apparatus: Electric field specificity and insulation design concept. *IEEE Electr. Insul. Mag.* **2002**, *18*, 27–36. [CrossRef]